Xinjie. 2015. *Int. J. Vehicle Structures & Systems*, 7(2), 66-70
ISSN: 0975-3060 (Print), 0975-3540 (Online)
doi: 10.4273/ijvss.7.2.04

International Journal of Vehicle Structures & Systems
Available online at www.ijvss.maftree.org

Computational Fluid Dynamics Analysis and Runner Test of Automobile Engine Intake Manifold Structure

Zhang Xinjie

Qingdao Agricultural University, Qingdao Shandong, China
Email: zhxj200481@126.com

ABSTRACT:

Computational fluid dynamics analysis for three intake manifold schemes were carried out by STAR-CCM software to obtain the velocity field, pressure field and pressure loss equilibrium. Based on the simulation results, the best scheme was chosen to verify and validate the numerical results through a runner test. The simulation and test results helped the designer to accurately find the unreasonable section of intake manifold with a view to re-design or apply minor modifications followed by re-analysis of the intake manifold which can reduce the number of experiemental tests.

KEYWORDS:

Engine intake manifold; Computational fluid dynamics; Pressure loss; Flow analysis; Runner test

CITATION:

Z. Xinjie. 2015. Computational Fluid Dynamic Analysis and Runner Test of Automobile Engine Intake Manifold Structure, *Int. J. Vehicle Structures & Systems*, 7(2), 66-70. doi:10.4273/ijvss.7.2.04

1. Introduction

The intake manifold structure is an important part of the intake system in automobile engine. Its size, shape and arrangement have greater influence on the outlet flow, intake resistance & efficiency, whole engine power, economy and emission [1-2]. So the design of intake manifold structure becomes an important aspect in the automobile engine design. There are many influencing factors in the intake system of the engine. The intake resistance and resonant induction have relatively large influence on the volumetric efficiency and intake loss of engine [3-4]. Although the intake process is a dynamic process, the flow resistance data obtained under steady-state conditions can judge the quality of intake system design [5]. Hence, steady state flow analysis of the entire intake system including the inlet and pressure stabilized cavity before and after the change was carried by using numerical methods. The change of flow resistance coefficient was used to assess the performance of engine and manifold volumetric efficiency. This approach is equivalent to the flow resistance test of the intake system on the steady flow simulation bench such that the calculated results can be compared with the experimental results. In previous work [6], finite element simulation was used to design and optimize a plastic manifold structure. In this paper, computational fluid dynamic (CFD) analyses for the intake manifold structure for three different schemes were carried out. The optimal scheme was chosen by comparing the pressure field, velocity field and pressure loss equilibrium. The optimal scheme was validated through runner test.

2. Theoretical model

The gas flow is mainly controlled by the laws of conservation of mass, conservation of momentum and conservation of energy. If there is an interaction between the group elements in the flow, the flow must abide by the law of conservation of component. If it is a turbulent state, the system should comply with the turbulent transport. The law of conservation of mass is given by,

$$\frac{\partial \rho}{\partial t} + div(\rho \vec{u}) = 0 \quad (1)$$

The law of conservation of momentum is given by,

$$\frac{\partial(\rho u)}{\partial t} + div(\rho u \vec{u}) = -\frac{\partial p}{\partial x} + \frac{\partial \tau_{xx}}{\partial x} + \frac{\partial \tau_{yx}}{\partial y} + \frac{\partial \tau_{zx}}{\partial z} + F_x \quad (2)$$

$$\frac{\partial(\rho v)}{\partial t} + div(\rho v \vec{u}) = -\frac{\partial p}{\partial y} + \frac{\partial \tau_{xy}}{\partial x} + \frac{\partial \tau_{yy}}{\partial y} + \frac{\partial \tau_{zy}}{\partial z} + F_y \quad (3)$$

$$\frac{\partial(\rho \omega)}{\partial t} + div(\rho \omega \vec{u}) = -\frac{\partial p}{\partial y} + \frac{\partial \tau_{xz}}{\partial x} + \frac{\partial \tau_{yz}}{\partial y} + \frac{\partial \tau_{zz}}{\partial z} + F_z \quad (4)$$

The law of conservation of energy is given by,

$$\frac{\partial(\rho T)}{\partial t} + div(\rho \vec{u} T) = div\left(\frac{k}{c_p} grad\, T\right) + S_T \quad (5)$$

Where P is pressure on the micro body of fluid, τ_{xx}, τ_{xy} and τ_{xz} is the viscous force component on the micro body surface due to molecular viscosity, F_x, F_y and F_z is the volume force on the micro body, C_p is specific heat capacity, T is temperature, k is heat transfer coefficient of fluid and S_T is the internal heat source of fluid. k−ε equation based on isotropic hypothesis has the characteristics of high stability calculation requiring less computing resources. RNGk−ε model can remove small scale motion from the equation systematically, and better treat the flow with high strain rate and has large streamline bending degree [7]. Hence, RNGk−ε turbulence model was chosen in this paper.

3. Grid model and boundary conditions

According to the intake manifold size, shape and location, three design schemes of intake manifold structure were considered. Fig. 1 shows the intake runner design schemes and their cross section views. Intake manifold structure material was PA66 + 35%GF with elastic modulus as 2250MPa (150°C, RH0), Poisson's ratio as 0.33, density as 1410 kg/m^3 and thermal expansion coefficient as 3.3×10^{-5} m/m/ºC. Steady state time model was considered. The temperature change, heat transfer and thermal radiation were considered in the thermal model. High Reynolds number mode was set for the turbulence model. Incompressible air was considered as single-phase fluid with three dimensional flow. Its thermal effect was not considered due to the friction between fluid and wall. Gas at the intake was assumed to be in a turbulent state. The flow field was assumed as constant temperature without energy transfer. The gas phase was air under normal temperature. The physical properties of gas flow are given in Table 1. FAME grid was used for meshing. The boundary layer was set as 2 layers. Grid was properly encrypted in high velocity region. There were 175000 elements for a chosen mesh size of 2mm. The grid models of three schemes are shown in Fig. 2. SMPISO algorithm with relaxation factor of the calculated physical quantities was considered as solver algorithm with upwind difference scheme.

Table 1: Physical properties of gas

Parameter	Temp., T(°C)	Mass flow, ρ (kg/s)	Press., P (Pa)	Viscosity, μ (Pa.s)
Flow-by-gas	23	0.11	101325	2.09×10^{-5}

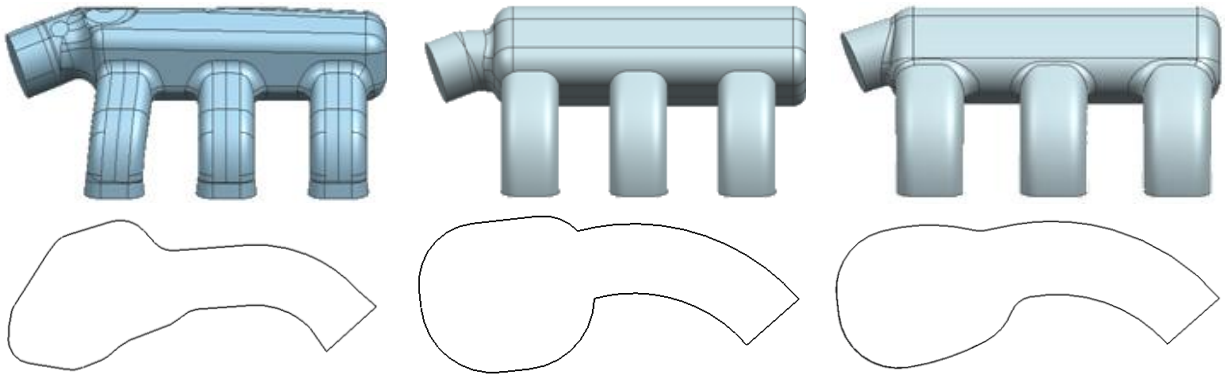

Fig. 1: Intake manifold runner designs overview (top) and cross-section (bottom); Scheme 1 (Left), 2 (Middle) & 3 (Right)

Fig. 2: Intake manifold runner grid models for scheme 1 (Left), 2 (Middle) & 3 (Right)

4. Simulation results & discussions

Smooth air-intake, small pressure loss and good equilibrium between each cylinder (<5%) were required for intake manifold design. CFD analysis was carried out using STAR+CCM software [8]. The optimal design plan was determined by comparing the velocity field, pressure field and pressure loss. The velocity field distribution of three design schemes of intake manifold were shown in Fig. 3 to Fig. 5. Flow velocity of all three schemes at intake was 0.11m/s. In scheme one, the flow velocity in throttle inlet and plenum chamber was uniform without large whirlpool. Whilst in the runner turning area, the flow velocity has increased. In scheme 2, flow velocity in throttle inlet, plenum chamber and runner turning area was uniform without large whirlpool. The overall fluidity was good. In scheme 3, flow velocity in throttle inlet and plenum chamber was uniform without large whirlpool. In the runner corner and connection between runner and plenum chamber, the flow velocity has increased.

The pressure field distribution of three design schemes of intake manifold were shown in Fig. 6 to Fig. 8. In scheme 1, when each runner was open, the pressure in plenum chamber was more balanced without obvious mutation site. In the connection between the runner and plenum chamber, pressure change was not obvious. In scheme 2, when each runner was open, the pressure in the plenum chamber and the connection between runner and plenum chamber runner were all balanced without obvious mutation site. In scheme 3, when each runner was open, the pressure in the plenum chamber was balanced without obvious mutation site. In the connection between runner and plenum chamber, the pressure change was obvious. In the positions marked by arrows for schemes 1 and 3, the pressure change and flow velocity variation were larger because the bending radius of intake manifold in this site was larger.

The pressure loss of each runner was determined by the following formula when the given flow rate:

$$\Delta P_Q = P_1 + 0.5\rho\left(4Q/\pi D_1^2\right)^2 - P_2 + 0.5\rho\left(4Q/\pi D_2^2\right)^2 \quad (6)$$

Where P_1 is the static pressure of inlet, P_2 is the static pressure of outlet, Q is airflow, ρ is air density, D_1 and D_2 are the inlet and outlet diameters. Pressure loss equilibrium analysis results of three schemes were summarised in Table 2. For scheme 1, the equilibrium was poor with overall pressure loss equilibrium range of 11.92% - 16.12%. The equilibrium for Scheme 3 had improved from the scheme 1 with the overall pressure loss equilibrium range of 4.09% - 5.89%. The intake resistance of runner 1 was large for schemes 1 and 3. For scheme 2, the flow velocity was uniform with better overall fluidity and the internal pressure equilibrium was more. There were no major pressure jump and the pressure loss range is 2.91% - 2.14%. Hence, scheme 2 was selected for manufacturing trial and runner test.

Table 2: Pressure loss equilibrium analysis result of scheme one

Press. loss (Pa)	Runner 1	Runner 2	Runner 3	Average
Scheme 1	1528	1145	1422	1365
Scheme 2	1510	1436	1456	1467
Scheme 3	2492	2304	2548	2448

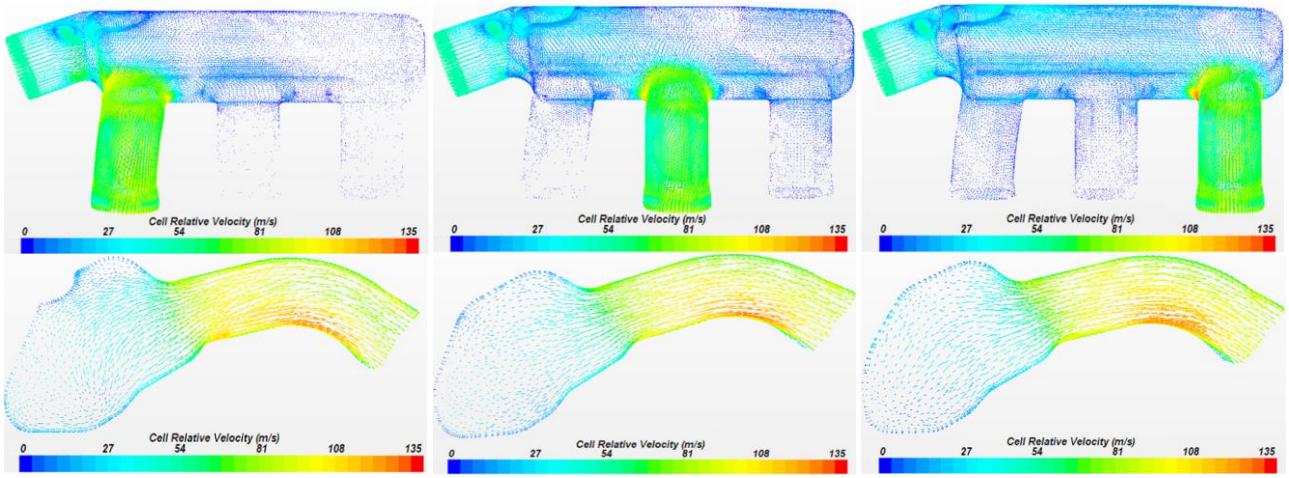

Fig. 3: Velocity field for Scheme 1 of intake manifold - overview (top) and cross-section (bottom); Runner 1 (Left), 2 (Middle) & 3 (Right)

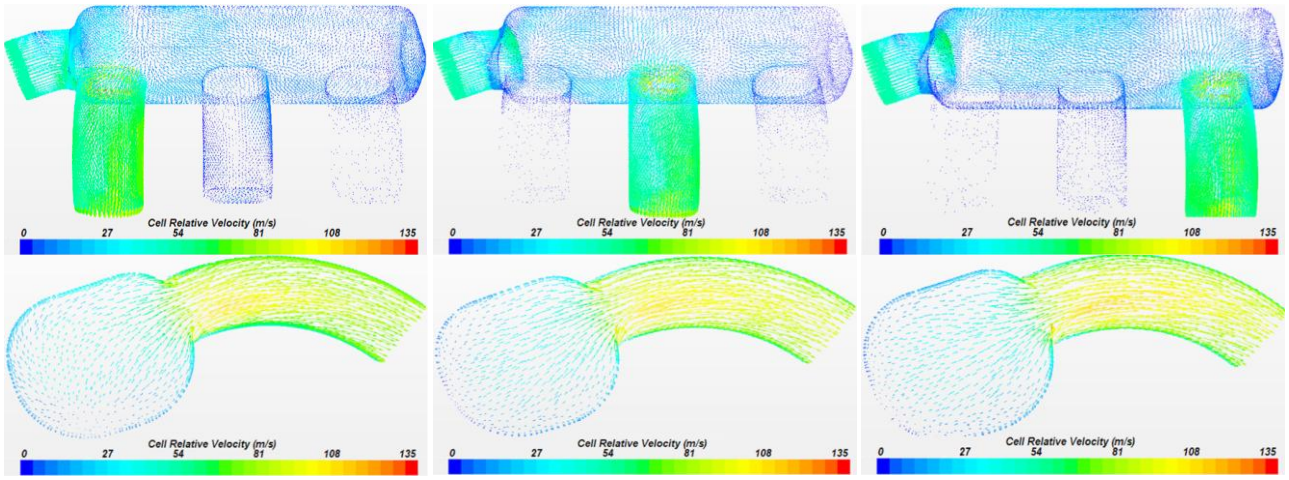

Fig. 4: Velocity field for Scheme 2 of intake manifold - overview (top) and cross-section (bottom); Runner 1 (Left), 2 (Middle) & 3 (Right)

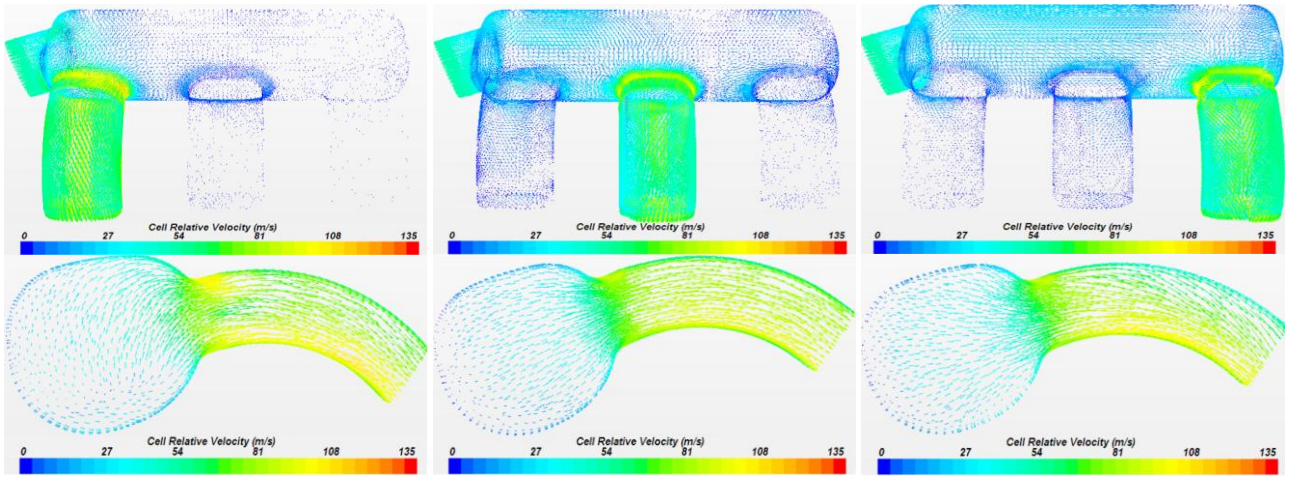

Fig. 5: Velocity field for Scheme 3 of intake manifold - overview (top) and cross-section (bottom); Runner 1 (Left), 2 (Middle) & 3 (Right)

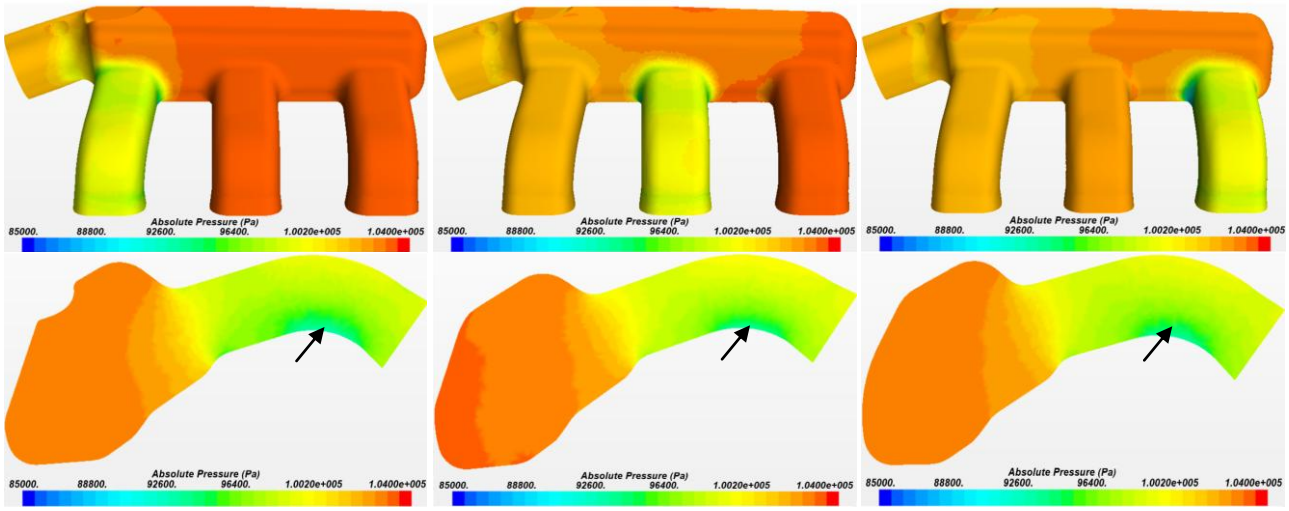

Fig. 6: Pressure field for Scheme 1 of intake manifold - overview (top) and cross-section (bottom); Runner 1 (Left), 2 (Middle) & 3 (Right)

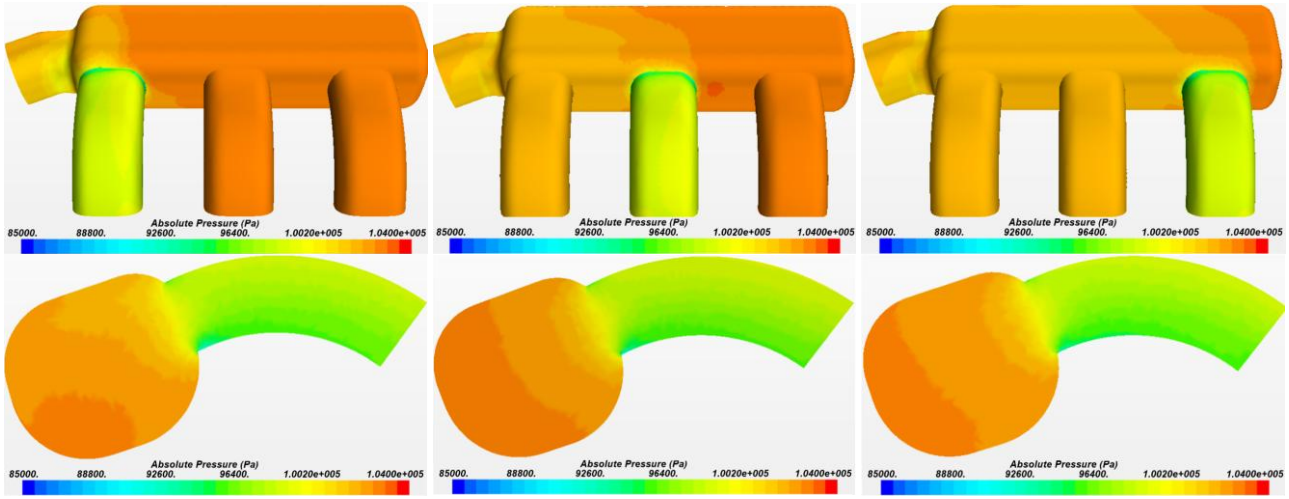

Fig. 7: Pressure field for Scheme 2 of intake manifold - overview (top) and cross-section (bottom); Runner 1 (Left), 2 (Middle) & 3 (Right)

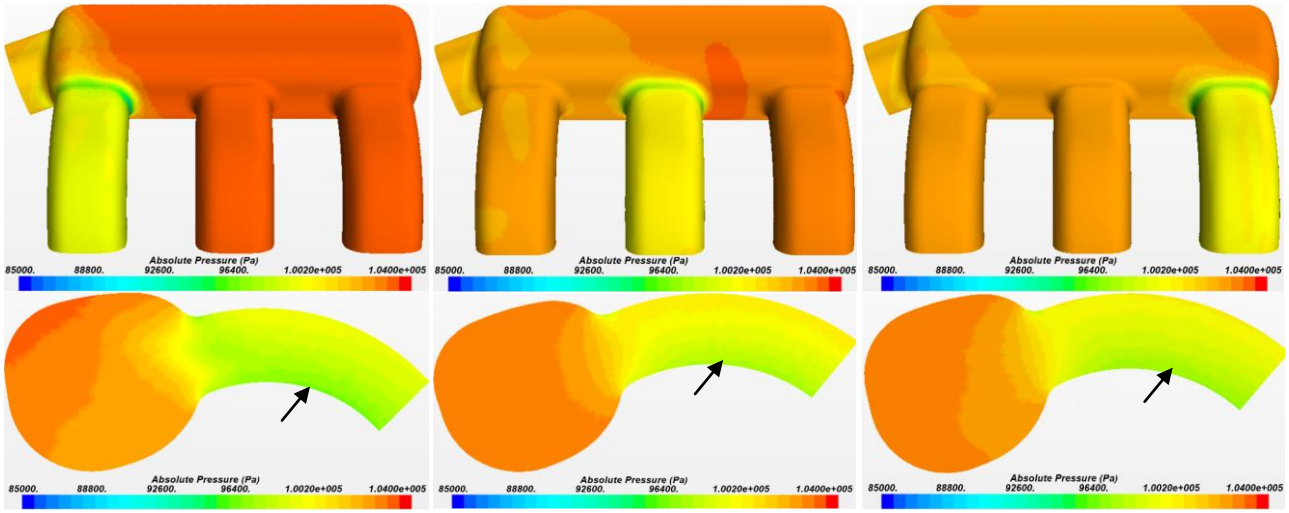

Fig. 8: Pressure field for Scheme 3 of intake manifold - overview (top) and cross-section (bottom); Runner 1 (Left), 2 (Middle) & 3 (Right)

5. Intake manifold runner test

Intake manifold runner test based on steady flow was carried out on the test bench. A schematic diagram of runner test bench is shown in Fig. 9. The pressure was obtained using a sensor at the entry of intake manifold. The flow meter was positioned between manifold and fan and thereby the pressure at exit can be measured. In runner test, the cylinder liner of 30mm in diameter was chosen. Fig. 10 shows a photograph of the intake manifold runner test using the scheme 2 prototype. Constant flow conditions were set by computer. Pressure data from the runner test was gathered by computer based acquisition system. Pressure loss equilibrium obtained from the test and CFD simulation are in good agreement as shown in Table 3.

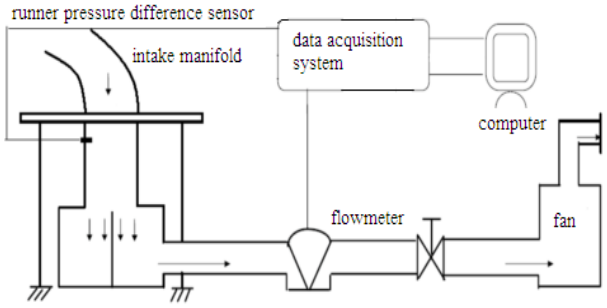

Fig. 9: Schematic diagram of intake manifold runner test bench

Fig. 10: Intake manifold runner test case

Table 3: Scheme 2 pressure loss - Runner test vs. CFD analysis

Press. loss (Pa)	Runner 1	Runner 2	Runner 3	Average
Runner test	1615	1493	1589	1562
CFD analysis	1510	1436	1456	1467

6. Conclusions

Flow characteristics of intake manifold was analyzed by CFD software STAR-CCM+. In this paper, velocity field and pressure field pressure loss for three different designs of manifold structure were post-processed from the simulation to down-select the best scheme. The maximum uniformity of pressure loss of the best scheme (#2) was 4.8%, which was within the reasonable range. The accuracy of the simulation model was verified though a runner test of intake manifold. The results from simulation and runner test were paired well for each runner #1 to #3. The three-dimensional flow field in the intake manifold structure can be obtained through CFD simulation. Thus, simulation results provided certain theoretical basis for the design and development of intake manifold which can reduce number of tests and shorten the product development cycle.

REFERENCES:

[1] J. Galindoa, J.M. Lujána and J.R. Serrano. 2004. Design of an exhaust manifold to improve transient performance of a high-speed turbocharged diesel engine, *J. Experimental Thermal & Fluid Science*, 28, 863-875. http://dx.doi.org/10.1016/j.expthermflusci.2004.01.003.

[2] A.S. Green and T. Moumtzis. 2002. Case study: Use of inlet manifold design techniques for combustion applications, *J. Applied Thermal Engg.*, 22, 1519-1527. http://dx.doi.org/10.1016/S1359-4311(02)00070-4.

[3] N. Ling, X. Wei and B. Minli. 2011. CFD simulation of inlet manifold modification design, *J. Liaoning Technical University (Natural Science)*, 1, 1-2.

[4] D. Chalet and P. Chesse. 2010. Fluid dynamic modeling of junctions in internal combustion engine inlet and exhaust systems, *J. Thermal Science*, 19, 410-418. http://dx.doi.org/10.1007/s11630-010-0402-0.

[5] Y. Li, W. Weimin and C. Zhiqiang. 2009. CFD analysis and improvement of intake manifold for a gasoline engine, *CDAJ-China*, 1-6.

[6] Z. Xinjie. 2013. Finite element simulation for improved design of plastic intake manifold for four cylinder engines, *Int. J. Vehicle Structures & Systems*, 5(3-4), 105-108. http://dx.doi.org/10.4273/ijvss.5.3-4.05.

[7] P. Dittrich and H. Reister. 1995. Turbulent flow in an intake manifold, *J. Forschung Im Ingenieurwesen*, 61, 195-200. http://dx.doi.org/10.1007/BF02609484.

[8] M. Sekavcnik, T. Ogorevc and L. Skerget. 2005. CFD analysis of the dynamic behavior of a pipe system, *J. Forshung Im Ingenieuruesen*, 70, 139-144. http://dx.doi.org/10.1007/s10010-006-0024-6.